Fatigue performance of shelled additively manufactured parts subjected to hot isostatic pressing

Anton du Plessis[1,2,3], Seyed Mohammad Javad Razavi [4], Di Wan [4], Filippo Berto [4], Adam Imdaadulah [3], Chad Beamer [5], James Shipley [6], Eric MacDonald [7]

[1] Research group 3DInnovation, Stellenbosch University, Stellenbosch 7602, South Africa

[2] Department of Mechanical Engineering, Nelson Mandela University, Port Elizabeth 6001, South Africa

[3] Centre for Rapid Prototyping and Manufacture, Central University of Technology, Bloemfontein 9300, South Africa

[4] Department of Mechanical and Industrial Engineering, Norwegian University of Science and Technology, Richard Birkelands vei 2b, Trondheim, Norway

[5] Quintus Technologies LLC, 8270 Green Meadows Drive North, Lewis Center, OH 43035, United States

[6] Quintus Technologies AB, Västerås, Sweden

[7] University of Texas at El Paso, TX 79968, United States

Additive manufacturing (AM) of metal components is increasingly used in high performance applications, especially in the aerospace industry. Laser powder bed fusion (L-PBF) of metals is the most widely used and mature process for this purpose, but it comes with some challenges. One of these challenges involves manufacturing quality and associated mechanical properties that can be negatively influenced by the presence of process-induced porosity, directional microstructure, residual stress and more. Hot isostatic pressing (HIP) has emerged as a key technology for post-processing such components, acting to improve the mechanical properties and especially the fatigue properties. This process is often required as a routine and mandatory step to ensure metal AM components can be used for critical applications and to mitigate potential manufacturing problems. It has recently been demonstrated that metal AM components can be manufactured through printing of a shell only – therefore with process powder remaining enclosed in the part – whereby the subsequent HIP cycle fully densifies the material. This approach has some advantages, including primarily a reduction in laser processing time during the L-PBF process, acting to reduce total costs. In this present work, the fatigue performance of this hybrid L-PBF and HIP process is investigated, in comparison to the equivalent solid processing route.

Key words: additive manufacturing; laser powder bed fusion; hot isostatic pressing; fracture; fatigue

1. Introduction

Metal additive manufacturing (AM) has emerged as a key manufacturing technology for the production of high-performance components in aerospace, automotive, medical and other industries [1–3]. Laser powder bed fusion (L-PBF) is the most widely used metal AM process for this purpose, and allows highly complex components to be produced with short lead times [4]. The design freedom allows unique structures to be manufactured with optimized geometries and improved properties compared

to traditionally manufactured components. Other advantages include the ability to minimize the number of components by combining or consolidating different parts and in the process reducing brazed/welded joints and material use. The short lead times are beneficial for low-volume production and for design iterations. High volume production is also possible, with advantages of unique geometries and material properties.

The quality of metal parts produced by L-PBF is influenced by many user-defined process parameters and potential external influences, which can potentially lead to reduced performance in the produced part/s. An example is the formation of porosity, especially when this is clustered in specific locations in the parts. The formation of porosity in L-PBF has been widely studied and is now well understood, including its effect on mechanical performance, acting as crack initiators in fatigue loading [5–8]. Unique microstructures may develop due to the repeated heating and cooling cycles, combined with the rapid solidification process. This typically leads to fine microstructures with elongated grains following the build direction, leading to anisotropy. Other important effects may include excessive and varied residual stress, micro-crack formation, oxidation, or unique surface roughness conditions varying across the part [9,10]. These issues can all be solved by careful process optimization, quality control and appropriate post-processing tools. For example, stress-relief heat treatment is widely acknowledged for its removal of residual stress of parts produced by L-PBF. Further heat treatments may improve the microstructure, by offering a path to recrystallize the grain structure while removing the directionality and hence reducing anisotropy [11].

If processes have been optimized and sufficient effort was made in quality control, the produced parts can reach mechanical properties the same or better than traditionally manufactured parts [2,12]. There has been a lot of concern in the past with respect to fatigue performance of AM parts due to high scatter in the results of reported research efforts [7,12–15], but by minimizing defects and optimizing microstructure and surface conditions, high fatigue performance can be achieved [7,13]. In order to ensure these properties, various qualification efforts have been reported with standards under development [16,17].

Despite the qualification efforts, there remains some possibility for reduced performance due to unexpected errors in the process. In order to safeguard against this possibility, hot isostatic pressing (HIP) has been widely adopted as a post-processing method for AM parts when their properties are critically important [7,18,19]. HIP is a process that combines a heat treatment with high applied pressure of an inert gas [11]. This serves to simultaneously close porosities, remove residual stresses, mitigate anisotropy and improve the microstructure and thereby improve the properties of the material [20–26]. Effectively, HIP acts to mitigate possible errors while having a beneficial impact on the properties of the parts. For example, for Ti6Al4V produced by L-PBF, the ductility increases from 5-10% (as built or stress relieved state) up to 15-20% (after HIP) with only a small reduction in yield strength [27]. Considering the internal defects as stress raisers in the fabricated part, their elimination or reduction of size directly impacts the fatigue properties of the L-PBF parts. Significant improvement of fatigue properties after HIP treatment has been reported in the literature by reducing the data scatter and thus increasing the design allowables [28–30]. It should be stated that this process targets the fully enclosed pores within the material and does not affect the surface defects or sub-surface defects connected to the surface (open porosities), therefore, in cases with as-built surface conditions where the fatigue crack initiates from the surface defects, removal of the internal defects using HIP will only have a minor or negligible impact on the fatigue properties [31–33]. On that account, the HIP process is recommended for cases where other surface treatments are used for elimination of surface defects. Nevertheless, there is an interest in utilizing as-built surface conditions for complex parts where some surfaces are not easily reached for processing, hence the interest and need to understand the properties of material in the as-built surface condition (with rough surfaces).

With the wide adoption of the HIP process subsequent to L-PBF, a new opportunity emerged to reduce the total manufacturing time and thereby reduce costs. One such approach has been demonstrated recently whereby fast scanning during the L-PBF process reduced the manufacturing time of components, with the associated lack of fusion porosity being healed by the subsequent HIP cycle [34]. This simple solution allows increased productivity, but excessive porosity is formed due to the high scan speed, and especially those connected to the surface are not healed by HIP as demonstrated in [21]. In addition, such process parameters reduce the surface quality which have a detrimental influence on the fatigue performance. Another approach was demonstrated in [35], where it was shown that it is possible to manufacture shelled geometries (dense shells with entirely enclosed powder), and a subsequent HIP cycle fully densifies this structure. This method was first demonstrated in 1999 in a proof of concept with 2.5 mm shell thickness for a small cylindrical component [36]. Other researchers have used the concept of manufacturing a shell or "can" and then removing powders and adding different powders for HIP processing, to create multi-material composites or new alloys [37].

In the present approach, the same powder used in the L-PBF powder bed (the unmolten powder) is ~~closed into the~~ entirely enclosed by a L-PBF manufactured shell and subsequently subjected to HIP for densification. The densification is associated with some shrinkage, which can be pre-compensated by simulation. The main advantage is the L-PBF processing time that can be reduced by an order of magnitude for large bulky parts. The quasi-static mechanical properties of this hybrid L-PBF and HIP process is identical to that of the regular L-PBF and HIP combination as demonstrated in prior work for Ti6Al4V [35]. The current work extends this evaluation to the fatigue performance of this material, and the shell is key to this performance as near-surface pores (in shell region) are more likely stress raisers than internal pores. This study includes microstructural and fracture surface analysis and discusses the reasons for the observed properties.

2. Materials and methods

Specimens were manufactured in Ti6Al4V using L-PBF, in vertical orientation and evaluated without surface post-processing, in other words the as-built surface condition was evaluated here. The reasoning behind this is to motivate for the use of such parts with complex geometries which cannot always be surface-processed. Ti6Al4V (ELI) powder (grade 23) from EOS with particle size distribution values of D_{10} =18µm, D_{50} =38µm and D_{90} =50µm was used. The L-PBF process was used to ~~with a D90 value of 50µm powder was used~~ to build the specimens under inert conditions on an EOS M290 system using the following optimized process parameters (EOS recommended parameters): laser power 280 W, scan speed 1.2 m/s, 0.03 mm layer height, hatch spacing 0.14 mm with 67 degrees rotation of hatch direction on each layer. The specimens were prepared using Materialise Magics software and sliced using EOSPRINT software. Three identical sets of specimens were built, two with solid geometries and one with shelled geometries with 1.5 mm shell thickness and internal fillets in internal cavity corners, to improve manufacturability, similar to previous work reported in [35]. Figure 1 illustrates an example of the fatigue hourglass shelled geometry. Due to the hourglass geometry and the central diameter of 6 mm coupled with shell thickness of 1.5 mm, the central powder cavity is 3 mm wide.

Formatted: Left

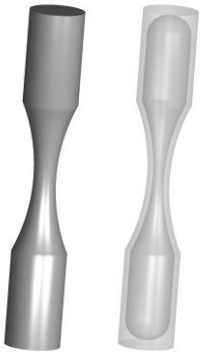

Figure 1: Fatigue hourglass specimen geometry shown with solid view (left) and shelled geometry and internal cavity visible in the transparent view – central cavity is 3 mm wide in 6 mm gauge diameter at narrowest section.

All samples were stress relieved in a vacuum furnace for 3 hours at 650 °C~~degrees~~, prior to removal from the baseplate. Subsequently the shelled batch and one solid batch of samples were annealed in a regular 2 hour annealing soak at 940 °C~~degrees~~, also in the vacuum furnace. An additional set of solid samples underwent a failed annealing cycle, with only 45 minutes of soak, followed by fast cooling and later fast temperature rise and further soak. This failed cycle was unplanned and could lead to unwanted microstructure development, but it was considered interesting for this study and was added here to supplement the work. ~~This provides some indication of robustness of the presented approach.~~

Hot isostatic pressing was performed at Quintus Techno~~l~~logies AB (Sweden), using the standard HIP cycle for Ti6Al4V cast material which is also common for AM produced components, i.e. 100 MPa Argon applied with 920 °C ~~degrees Celsius~~ for 2 hrs soak time followed by uniform rapid cooling (URC®, ~150 °C~~degrees~~ per minute). The shrinkage of the shelled hourglass fatigue sample is shown in Figure 2, and in the centre of the gauge section the total diameter reduced from 6 mm to 5.7 mm, which was incorporated into calculations for fatigue SN curves. A summary of all samples and their processing and testing conditions are provided in Table 1. The heat treatment and HIP parameters were selected based on typically used procedures. In a final application, the annealing heat treatment could be omitted.

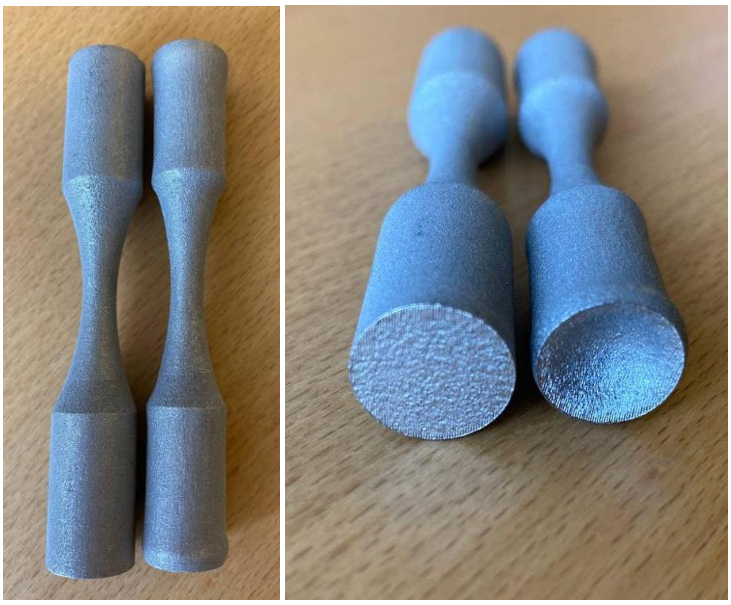

Figure 2: Comparison of solid and shelled geometries subsequent to HIP – shrinkage of shelled geometry is visible.

Table 1: Summary of samples and processing conditions in this study

	Terminology used	Stress relief	Annealing only	Anneal + HIP
Shelled set	SHELL	All – 18 samples	none	18 samples
Solid set 1	SOLID	All – 18 samples	9 samples	9 samples
Solid set 2	~~WHT~~ FHT (~~Wrong~~ Failed Heat Treatment)	All – 18 samples	9 samples	9 samples

Metallography samples were extracted from the fabricated specimens to analyze the microstructure. The samples were ground down to 4000 grit and electropolished using a methanolic H_2SO_4 (1 mol/L) electrolyte [38] at 40 V for 60 s. Scanning Electron Microscopy (SEM) were then performed on the polished samples using Thermo Fisher Quanta^{TM}650 FEG with 20 kV accelerating voltage.

The fabricated specimens were tested under load controlled axial tensile fatigue loading with a ~~loading~~ frequency of 20 Hz and a loading ratio of R = 0.01. An average of nine specimens were tested for each testing case to capture the stress-life diagrams of different L-PBF specimens. For run-out condition, a fatigue limit of 2 million cycles was considered and in some cases the fatigue tests were continued after this limit (up to five million cycles) to evaluate near limit failure of the specimens. The broken specimens were then prepared for SEM analysis by ultrasonic cleaning in ethanol for five minutes. Failure mechanisms of the tested specimens were then evaluated by studying the fatigue initiation sites, fatigue fracture morphology at the initiation and propagation locations and the effect of shell design on these aspects.

3. Results and discussions

3.1. Microstructure

The microstructure of the L-PBF samples in ~~transversal~~ XY plane (i.e. plane perpendicular to the build direction, all coordinates are as prescribed in the ISO/ASTM 52900 standard) obtained from SEM are shown in Figures 3 and 4. In these figures, the aluminum-rich darker zones correspond to α and α' phase, while the vanadium-rich brighter zones correspond to β phase. The SEM images in Figure 3 illustrate the presence of basketweave α+β microstructure of SOLID and ~~WHT~~FHT samples. In both cases, the width of α lath is almost identical, indicating the minor effect of the change in the heat treatment condition of ~~WHT~~FHT samples on the resulting microstructure. Performance of the HIP process on the other hand resulted in a bimodal microstructure of the material. The HIPed samples illustrate presence of the primary basketweave structure of α and β phase together with α' decorations in between. The presence of α' phase in the HIPed materials is associated with the fast cooling of the specimens after the HIP process. The same microstructure was observed for both SOLID-HIP and ~~WHT~~FHT-HIP samples.

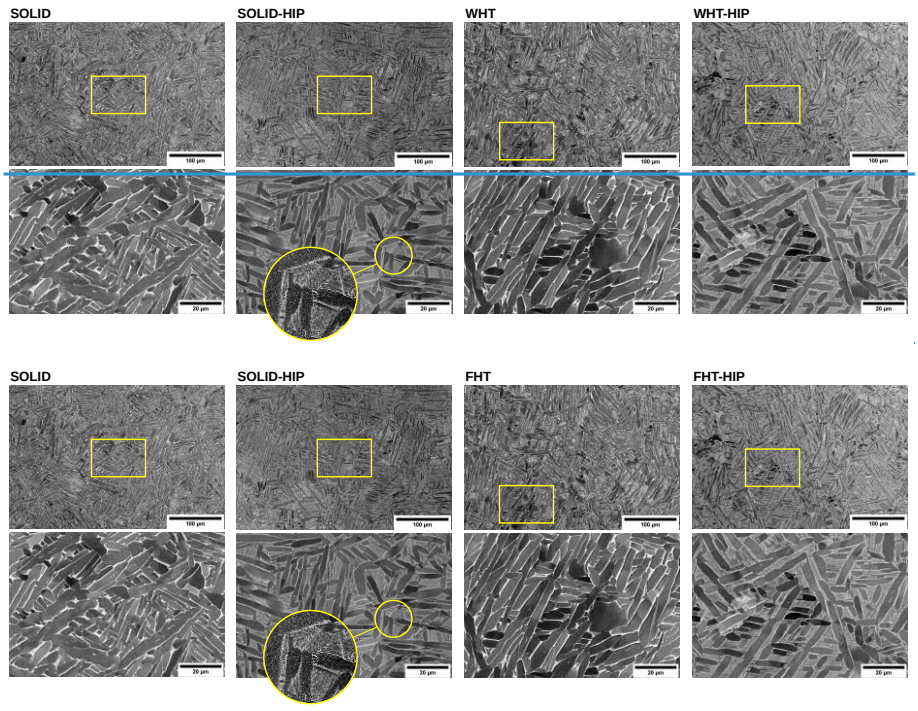

Figure 3: Scanning electron microscopic (SEM) analysis of the microstructures of SOLID and ~~WHT~~FHT samples prior and after HIP process. Higher magnification images of the microstructures are provided in the second row with the yellow~~red~~ rectangle showing the location where the image was taken.

Unlike the microstructure of solid specimens (both SOLID and ~~WHT~~FHT), where a uniform grain size and phase distribution was detected on the cross section of the samples, SHELL samples represented

a clear trace of the shell structure. According to Figure 4, two distinct types of microstructure can be observed in SHELL samples. The shell regions in these samples have a microstructure very similar to that of the HIPped samples mentioned before (basketweave α+β with α' decorations). While the inner region of the sample represents equiaxed α grains surrounded by β phase in presence of α' clusters within the region. Although the thickness and geometry of the AM parts have been reported to directly influence the resulting microstructure and mechanical properties [10,39], the use of annealing heat treatment and HIP process in this research have possibly eliminated the effect of this factor, resulting in the similar microstructure of the shell regions in SHELL samples and that of the SOLID samples. Unlike the other cases where no apparent porosity was detected, the inner area of the shell samples represented the presence of entrapped pores. The pore size was in a range of 0.7 to 15.7 µm with an average size of 4.9±~~+-~~3.6 µm. It should be mentioned that due to the edge effect of the electrochemical reactions, the internal pores can be corroded during electropolishing, and their size on the surface can be slightly overestimated. No clear indication of interfacial defects was observed in SEM analysis and the defects were mainly distributed uniformly within the inner region of the shell samples. The presence of small pores in the inner region is expected, since~~as~~ Argon is not soluble in Ti6Al4V and such entrapped HIPed pores have been previously observed to regrow after subsequent heat treatment [21,40]. In larger components, the relative shell thickness effect on the microstructure of the shelled components can be more pronounced when compared with solid parts of the same scale. This requires further investigation to clarify its level of dependency.

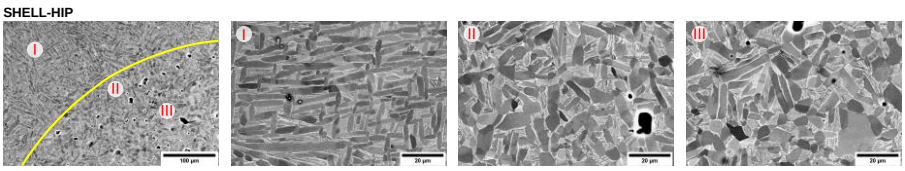

Figure 4: Scanning electron microscopic (SEM) analysis of the microstructures of SHELL samples after HIP process. Higher magnification images of the microstructures from different regions are provided; (I) shell region, (II) interface between shell and the inner area, and (III) inner area of the specimen (formed from the entrapped powders).

3.2. Fatigue strength

The main fatigue test results in the form of stress-fatigue life diagrams are shown in Figure 5. According to Figure 5a, the solid specimens that were subjected to annealing (SOLID) and ~~incorrect~~ failed annealing heat treatment (~~WHT~~FHT) show similar fatigue behavior having a fatigue strength of roughly 300 MPa at 10^6~~one million~~ cycles. This is especially true for higher load levels, while for lower load levels the SOLID specimens represent slightly higher fatigue strength (Figure 5a). Performing HIP on these two sets of specimens resulted in a limited improvement in fatigue strength especially in the higher number of cycles where the fatigue strength is highly dependent on the strength of the material (Figure 5b and 5c). The microstructural analysis revealed the absence of any internal pore in the fabricated parts (in the micrographs investigated), therefore, the observed variation is expected to be related to the change in the microstructure of the material after HIP process. As discussed in the previous section, the presence of martensitic α' phase in HIPed samples was verified. This phase is known for its limited ductility and high strength and the observed fatigue improvement can be associated to the presence of this phase rather than any impact due to the closure of the internal pores.

For the shelled-HIP samples~~tests~~ (Figure 5d), the performance is reduced reaching a fatigue strength at 10^6 cycles of just over 200 MPa. At this load level, one specimen ran out at $2x10^6$ cycles which is indicative of the reasonably good performance of these specimens. It is worth mentioning that the Shelled-HIP specimens had around 9.8% reduction of volume and 5.3% increase of surface to volume ration in the gauge area after shrinkage compared to the SOLID specimens. This higher surface to volume ratio can be considered as a potential source for lower fatigue strength of these samples when compared to the SOLID specimens. Similar observations were previously reported in [41] for L-PBF samples fabricated with different diameters.

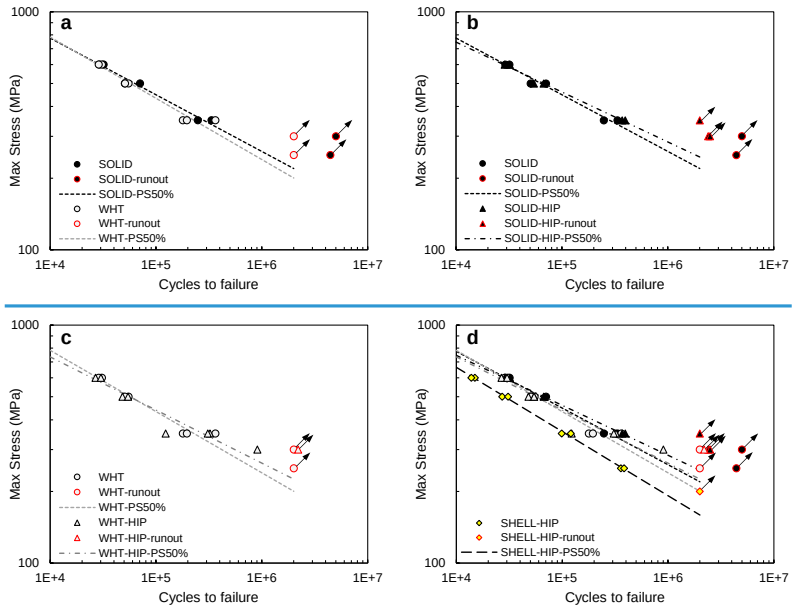

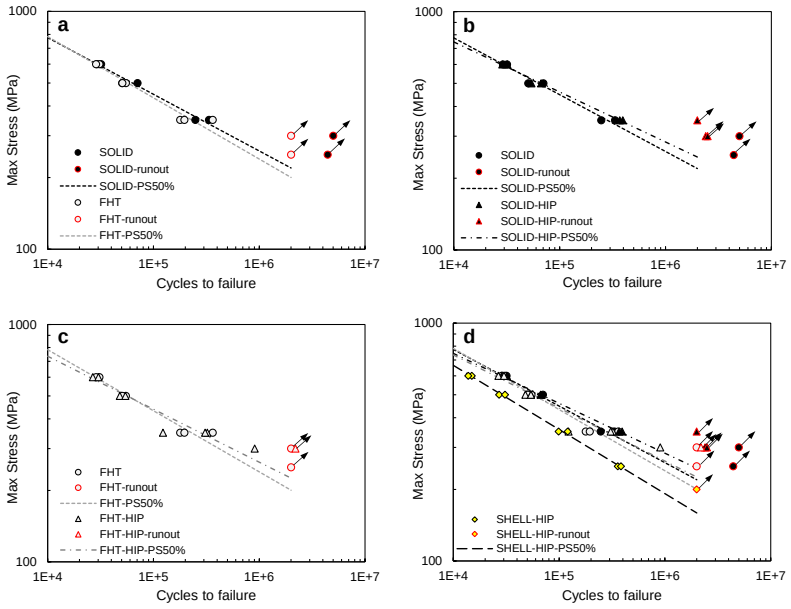

Figure 5: Comparative fatigue results of L-PBF Ti-6Al-4V specimens with different processing conditions, (a) SOLID and ~~WHT~~FHT, (b) SOLID and SOLID-HIP, (c) ~~WHT~~FHT and ~~WHT~~FHT-HIP, and (d) all tested specimens including SHELL-HIP. The dashed lines in the plots show 50% probability of survival for each case.

3.3. Failure assessment

Fractography was performed on the tested specimens to investigate possible differences in fatigue failure of the specimens with different processing conditions. Figure 6 represents a comparative representation of the fracture surface of SOLID, SOLID-HIP and SHELL-HIP specimens. The fracture surface ~~fracture~~ features of ~~WHT~~FHT and ~~WHT~~FHT-HIP specimens were similar to that of the other solid parts and for sake of brevity their results are not presented here. In all cases, the fatigue crack has initiated from the surface of the specimens, propagating through the net section of the specimens. No evidence of internal pores and sub-surface pores was detected in the solid specimens and in the shell area of the SHELL specimens. The fatigue crack initiation zone in all cases was identified by the microstructural ~~dependent~~ features on the fracture surface. A combination of inter-granular and trans-granular crack propagation along the α and β grains resulted in a tortuous fracture surface in this area with an observable pattern of basketweave microstructure. This stage was then followed by fatigue crack propagation. In the propagation stage, the microstructure-dependent tortuous features disappeared and the typical fatigue~~failure~~ striation was observed. In addition to the mentioned features, SOLID-HIP specimens show a higher presence of secondary cracks on the surface, which can be linked to the brittle α' phase in this condition.

A distinctive fracture surface was observed in the SHELL-HIP specimens. In these specimens, the shell area and the inner region of the specimens illustrated different fracture morphology. Details of fracture features in these specimens are shown in Figure 7. While the shell area was identified very similar to SOLID-HIP specimen, a transition from a smooth fatigue crack propagation surface to a

tortuous surface in the inner area was detected. By closer inspection of the fatigue features in the neighbouring area of the interface, both smooth and tortuous faces show fatigue striation indicating continuous fatigue propagation even in the inner region of the specimen. The difference in the morphology of this area is linked to the different microstructural features. As stated earlier, while the shell region is identified by basketweave α+β microstructure, equiaxed α grains were observed in the inner region of the SHELL-HIP samples. Besides, the residual porosities in this area can dictate the crack path and increase the tortuosity of the fracture surface.

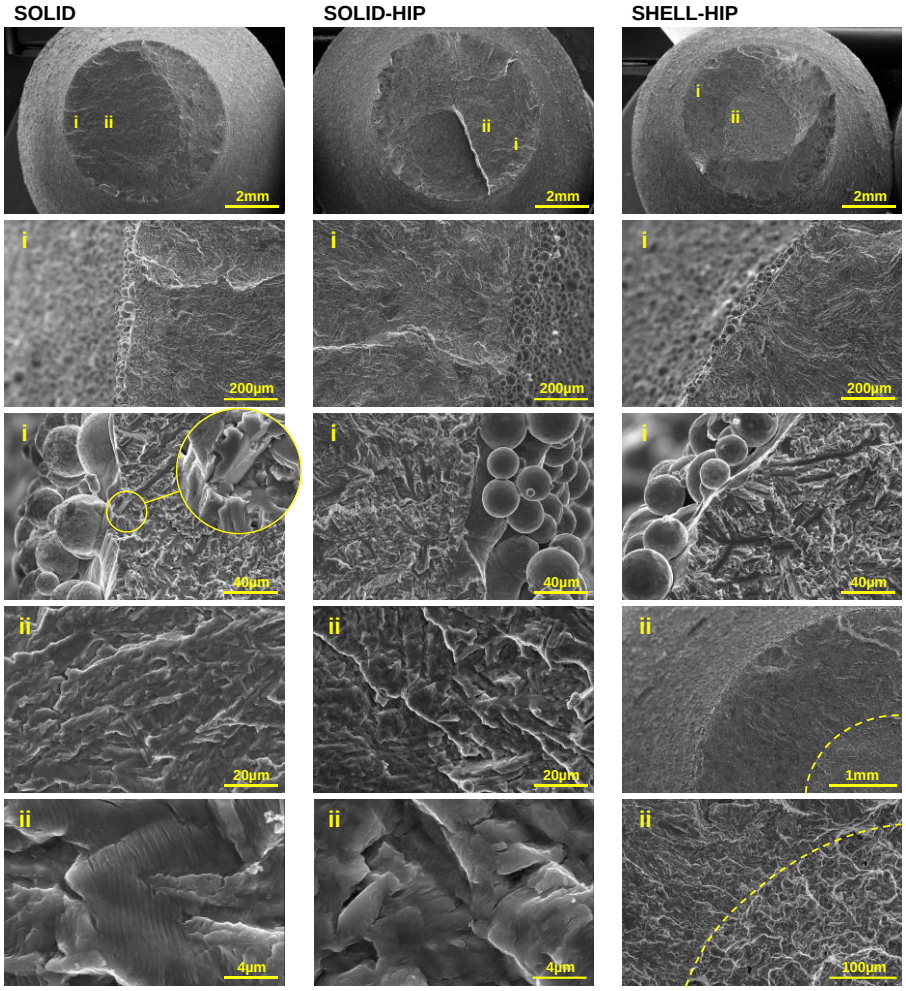

Figure 6: SEM fractographs of the fracture surface of the tested solid specimens with annealing (SOLID), and HIP (SOLID-HIP) post processing and shelled specimens subjected to both annealing and HIP (SHELL-HIP). Higher magnification images of fatigue initiation sites and fatigue propagation area are provided.

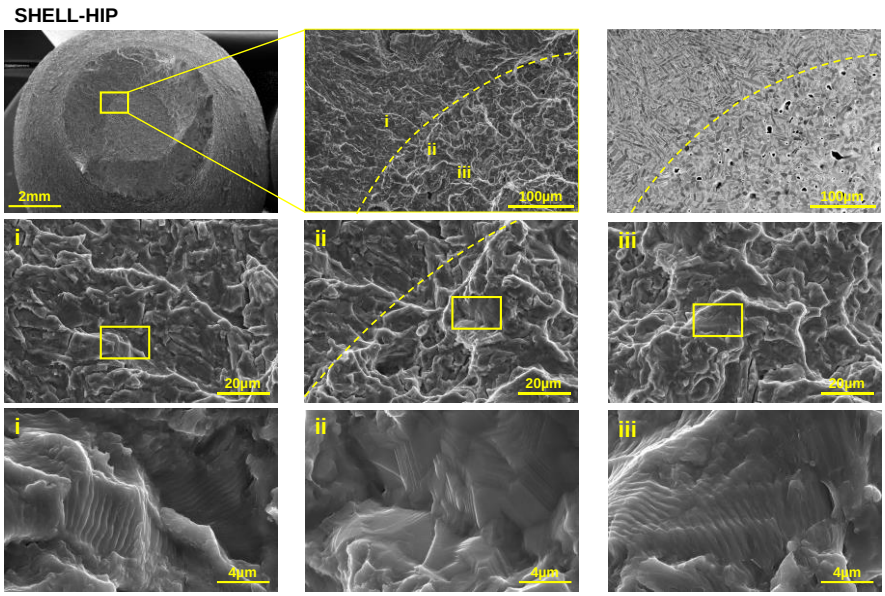

Figure 7: SEM fractographs of the fracture surface of the tested shelled specimens subjected to both annealing and HIP (SHELL-HIP). The image on the top right hand side illustrates the microstructure of the material in the studied region.

4. Conclusions

In this work, a detailed experimental study was performed on the fatigue performance of Ti6Al4V manufactured by L-PBF in as-built surface condition and heat treated according to both annealing and hot isostatic pressing. This was compared to a shelled manufacturing approach followed by the same processing steps, to evaluate the performance of parts manufactured by this faster hybrid approach.

The similar performance achieved for solid L-PBF samples in annealed state and in HIP state can be explained by defect free material (density-optimized~~good~~ process parameters) and ~~good~~ high ductility of the annealed material. Due to the similar temperatures used in the two types of treatments, the conventional heat treatment may be omitted to achieve the same microstructure and properties. ~~These results are useful as a reference for researchers interested in using this type of material.~~ The fatigue performance in this condition is likely mainly influenced by the surface condition as evidenced by fractography results, contributing to the similar performance obtained. The shelled-HIP samples show somewhat reduced performance with fatigue strength approximately 220 MPa compared to 300 MPa for solid samples, with a similar reduction % at various load levels. This reduction is not huge, but important to consider when using this approach for cyclic loading applications. The ability of this hybrid approach to produce material that reaches 2 x 10^6~~million~~ cycles under fatigue loading at 200 MPa is a notable achievement and may find particular applications. Nevertheless, the approach should be used with caution due to the reduced life compared to the solid processing route. Another important consideration is the possibility of increased local stresses for internal pores in the inner region, when

other loadings are used such as bending, or when the specimen geometry has a larger thickness variation than the current work. Such conditions could lead to reduced fatigue strength. Further future work is envisaged in optimizing the hot isostatic pressing process to enhance the performance for this hybrid process and specifically investigating the interface obtained between shell and interior. As fatigue performance in this type of material is mainly controlled by the crack initiation stage, the surface and near-surface region is most critical – i.e. the shell region. It is therefore reasonable to assume that further improved performance can be achieved by appropriate surface processing.

Acknowledgements

Funding of AdP through the South African Collaborative Program in Additive Manufacturing (CPAM) is thankfully acknowledged.

Statement on Conflicts of Interest

Two of the authors of this article are part of the editorial board of the journal. To avoid potential conflicts of interest, the responsibility for the editorial and peer-review process of this article lies with the other editors of the journal. Furthermore, the authors of this article were removed from the peer review process and have no access to confidential information related to the editorial process of this article.

References

[1] B. Blakey-Milner, P. Gradl, G. Snedden, M. Brooks, J. Pitot, E. Lopez, M. Leary, F. Berto, A. du Plessis, Metal additive manufacturing in aerospace: A review, Mater. Des. 209 (2021) 110008. https://doi.org/10.1016/J.MATDES.2021.110008.

[2] T. Debroy, H.L. Wei, J.S. Zuback, T. Mukherjee, J.W. Elmer, J.O. Milewski, A.M. Beese, A. Wilson-Heid, A. De, W. Zhang, Additive manufacturing of metallic components – Process, structure and properties, Prog. Mater. Sci. 92 (2018) 112–224. https://doi.org/10.1016/j.pmatsci.2017.10.001.

[3] I. Gibson, D. Rosen, B. Stucker, Additive manufacturing technologies: 3D printing, rapid prototyping, and direct digital manufacturing, second edition, 2015. https://doi.org/10.1007/978-1-4939-2113-3.

[4] I. Yadroitsev, I. Yadroitsava, A. Du Plessis, E. MacDonald, eds., Fundamentals of Laser Powder Bed Fusion of Metals - 1st Edition, Elsevier, 2021. https://www.elsevier.com/books/fundamentals-of-laser-powder-bed-fusion-of-metals/yadroitsev/978-0-12-824090-8 (accessed November 20, 2020).

[5] A. du Plessis, I. Yadroitsava, I. Yadroitsev, Effects of defects on mechanical properties in metal additive manufacturing: A review focusing on X-ray tomography insights, Mater. Des. 187 (2020). https://doi.org/10.1016/j.matdes.2019.108385.

[6] N. Sanaei, A. Fatemi, N. Phan, Defect characteristics and analysis of their variability in metal L-PBF additive manufacturing, Mater. Des. 182 (2019) 108091. https://doi.org/10.1016/j.matdes.2019.108091.

[7] N. Sanaei, A. Fatemi, Defects in Additive Manufactured Metals and Their Effect on Fatigue

Performance: A State-of-the-Art Review, Prog. Mater. Sci. (2020) 100724. https://doi.org/10.1016/j.pmatsci.2020.100724.

[8] A. Du Plessis, Porosity in laser powder bed fusion, in: Fundam. Laser Powder Bed Fusion Met., Elsevier, 2021: pp. 155–178. https://doi.org/10.1016/B978-0-12-824090-8.00007-X.

[9] R. Molaei, A. Fatemi, S.M.J. Razavi, F. Berto, Fatigue and Fracture of Additively Manufactured Metallic Materials, Ref. Modul. Mater. Sci. Mater. Eng. (2021). https://doi.org/10.1016/B978-0-12-822944-6.00010-4.

[10] S.M.J. Razavi, B. Van Hooreweder, F. Berto, Effect of build thickness and geometry on quasi-static and fatigue behavior of Ti-6Al-4V produced by Electron Beam Melting, Addit. Manuf. 36 (2020) 101426. https://doi.org/10.1016/j.addma.2020.101426.

[11] H. V. Atkinson, S. Davies, Fundamental aspects of hot isostatic pressing: An overview, Metall. Mater. Trans. A Phys. Metall. Mater. Sci. 31 (2000) 2981–3000. https://doi.org/10.1007/s11661-000-0078-2.

[12] J.J. Lewandowski, M. Seifi, Metal Additive Manufacturing: A Review of Mechanical Properties, Annu. Rev. Mater. Res. 46 (2016) 151–186. https://doi.org/10.1146/annurev-matsci-070115-032024.

[13] U. Zerbst, G. Bruno, J.Y. Buffière, T. Wegener, T. Niendorf, T. Wu, X. Zhang, N. Kashaev, G. Meneghetti, N. Hrabe, M. Madia, T. Werner, K. Hilgenberg, M. Koukolíková, R. Procházka, J. Džugan, B. Möller, S. Beretta, A. Evans, R. Wagener, K. Schnabel, Damage tolerant design of additively manufactured metallic components subjected to cyclic loading: State of the art and challenges, Prog. Mater. Sci. 121 (2021) 100786. https://doi.org/10.1016/j.pmatsci.2021.100786.

[14] A. Yadollahi, M.J. Mahtabi, A. Khalili, H.R. Doude, J.C. Newman, Fatigue life prediction of additively manufactured material: Effects of surface roughness, defect size, and shape, Fatigue Fract. Eng. Mater. Struct. 41 (2018) 1602–1614. https://doi.org/10.1111/ffe.12799.

[15] A. Yadollahi, N. Shamsaei, Additive manufacturing of fatigue resistant materials: Challenges and opportunities, Int. J. Fatigue. 98 (2017) 14–31. https://doi.org/10.1016/j.ijfatigue.2017.01.001.

[16] M. Seifi, M. Gorelik, J. Waller, N. Hrabe, N. Shamsaei, S. Daniewicz, J.J. Lewandowski, Progress Towards Metal Additive Manufacturing Standardization to Support Qualification and Certification, JOM. 69 (2017) 439–455. https://doi.org/10.1007/s11837-017-2265-2.

[17] J. Gumpinger, M. Seifi, N. Shamsaei, C. Seidel, R.W. Russell, Recent progress on global standardization, Fundam. Laser Powder Bed Fusion Met. (2021) 563–582. https://doi.org/10.1016/b978-0-12-824090-8.00021-4.

[18] S. Shao, M.J. Mahtabi, N. Shamsaei, S.M. Thompson, Solubility of argon in laser additive manufactured α-titanium under hot isostatic pressing condition, Comput. Mater. Sci. 131 (2017) 209–219. https://doi.org/10.1016/j.commatsci.2017.01.040.

[19] P. Li, D.H. Warner, J.W. Pegues, M.D. Roach, N. Shamsaei, N. Phan, Investigation of the mechanisms by which hot isostatic pressing improves the fatigue performance of powder bed fused Ti-6Al-4V, Int. J. Fatigue. 120 (2019) 342–352. https://doi.org/10.1016/J.IJFATIGUE.2018.10.015.

[20] J. Benzing, N. Hrabe, T. Quinn, R. White, R. Rentz, M. Ahlfors, Hot isostatic pressing (HIP) to achieve isotropic microstructure and retain as-built strength in an additive manufacturing titanium alloy (Ti-6Al-4V), Mater. Lett. 257 (2019) 126690. https://doi.org/10.1016/J.MATLET.2019.126690.

[21] A. du Plessis, E. Macdonald, Hot isostatic pressing in metal additive manufacturing: X-ray tomography reveals details of pore closure, Addit. Manuf. 34 (2020) 101191. https://doi.org/10.1016/j.addma.2020.101191.

[22] C. Cai, B. Song, P. Xue, Q. Wei, J.M. Wu, W. Li, Y. Shi, Effect of hot isostatic pressing procedure on performance of Ti6Al4V: Surface qualities, microstructure and mechanical properties, J. Alloys Compd. 686 (2016) 55–63. https://doi.org/10.1016/j.jallcom.2016.05.280.

[23] C. Cai, B. Song, P. Xue, Q. Wei, C. Yan, Y. Shi, A novel near α-Ti alloy prepared by hot isostatic pressing: Microstructure evolution mechanism and high temperature tensile properties, Mater. Des. 106 (2016) 371–379. https://doi.org/10.1016/j.matdes.2016.05.092.

[24] C. Cai, X. Gao, Q. Teng, M. Li, K. Pan, B. Song, C. Yan, Q. Wei, Y. Shi, A novel hybrid selective laser melting/hot isostatic pressing of near-net shaped Ti-6Al-4V alloy using an in-situ tooling: Interfacial microstructure evolution and enhanced mechanical properties, Mater. Sci. Eng. A. 717 (2018) 95–104. https://doi.org/10.1016/j.msea.2018.01.079.

[25] A. Kaletsch, S. Qin, S. Herzog, C. Broeckmann, Influence of high initial porosity introduced by laser powder bed fusion on the fatigue strength of Inconel 718 after post-processing with hot isostatic pressing, Addit. Manuf. 47 (2021) 102331. https://doi.org/10.1016/j.addma.2021.102331.

[26] J.R. Poulin, A. Kreitcberg, V. Brailovski, Effect of hot isostatic pressing of laser powder bed fused Inconel 625 with purposely induced defects on the residual porosity and fatigue crack propagation behavior, Addit. Manuf. 47 (2021) 102324. https://doi.org/10.1016/j.addma.2021.102324.

[27] P. Krakhmalev, A.M. Vilardell, N. Takata, 13 - Structural integrity I: static mechanical properties, Fundam. Laser Powder Bed Fusion Met. (2021) 349–376. https://www.sciencedirect.com/science/article/pii/B9780128240908000196.

[28] H. Masuo, Y. Tanaka, S. Morokoshi, H. Yagura, T. Uchida, Y. Yamamoto, Y. Murakami, Influence of defects, surface roughness and HIP on the fatigue strength of Ti-6Al-4V manufactured by additive manufacturing, Int. J. Fatigue. 117 (2018) 163–179. https://doi.org/10.1016/j.ijfatigue.2018.07.020.

[29] S. Leuders, T. Lieneke, S. Lammers, T. Tröster, T. Niendorf, On the fatigue properties of metals manufactured by selective laser melting – The role of ductility, J. Mater. Res. 29 (2014) 1911–1919. https://doi.org/10.1557/jmr.2014.157.

[30] V. Popov, A. Katz-Demyanetz, A. Garkun, G. Muller, E. Strokin, H. Rosenson, Effect of Hot Isostatic Pressure treatment on the Electron-Beam Melted Ti-6Al-4V specimens, Procedia Manuf. 21 (2018) 125–132. https://doi.org/10.1016/j.promfg.2018.02.102.

[31] A.H. Chern, P. Nandwana, T. Yuan, M.M. Kirka, R.R. Dehoff, P.K. Liaw, C.E. Duty, A review on the fatigue behavior of Ti-6Al-4V fabricated by electron beam melting additive manufacturing, Int. J. Fatigue. 119 (2019) 173–184. https://doi.org/10.1016/J.IJFATIGUE.2018.09.022.

[32] M. Kahlin, H. Ansell, J.J. Moverare, Fatigue behaviour of notched additive manufactured Ti6Al4V with as-built surfaces, Int. J. Fatigue. 101 (2017) 51–60. https://doi.org/10.1016/J.IJFATIGUE.2017.04.009.

[33] M. Kahlin, H. Ansell, J.J. Moverare, Fatigue behaviour of additive manufactured Ti6Al4V, with as-built surfaces, exposed to variable amplitude loading, (2017). https://doi.org/10.1016/j.ijfatigue.2017.06.023.

[34] D. Herzog, K. Bartsch, B. Bossen, Productivity optimization of laser powder bed fusion by hot isostatic pressing, Addit. Manuf. 36 (2020) 101494.

https://doi.org/10.1016/j.addma.2020.101494.

[35] A. Du Plessis, B. Yelamanchi, C. Fischer, J. Miller, C. Beamer, K. Rogers, P. Cortes, J. Els, E. MacDonald, Productivity enhancement of laser powder bed fusion using compensated shelled geometries and hot isostatic pressing, Adv. Ind. Manuf. Eng. 2 (2021) 100031. https://doi.org/10.1016/j.aime.2021.100031.

[36] S. Das, M. Wohlert, J.J. Beaman, D.L. Bourell, Processing of titanium net shapes by SLS/HIP, Mater. Des. 20 (1999) 115–121. https://doi.org/10.1016/S0261-3069(99)00017-5.

[37] R. Sebastian, K. Anke, B. Christoph, Tailor-Made Net-Shape Composite Components by Combining Additive Manufacturing and Hot Isostatic Pressing, Hot Isostatic Press. HIP'17. 10 (2019) 203–209. https://doi.org/10.21741/9781644900031-27.

[38] D. Wan, Y. Ma, B. Sun, S.M.J. Razavi, D. Wang, X. Lu, W. Song, Evaluation of hydrogen effect on the fatigue crack growth behavior of medium-Mn steels via in-situ hydrogen plasma charging in an environmental scanning electron microscope, J. Mater. Sci. Technol. 85 (2021) 30–43. https://doi.org/10.1016/J.JMST.2020.12.069.

[39] Y.H. Kok, X.P. Tan, N.H. Loh, S.B. Tor, C.K. Chua, Geometry dependence of microstructure and microhardness for selective electron beam-melted Ti–6Al–4V parts, Virtual Phys. Prototyp. 11 (2016) 183–191. https://doi.org/10.1080/17452759.2016.1210483.

[40] S. Tammas-Williams, P.J. Withers, I. Todd, P.B. Prangnell, Porosity regrowth during heat treatment of hot isostatically pressed additively manufactured titanium components, Scr. Mater. 122 (2016) 72–76. https://doi.org/10.1016/J.SCRIPTAMAT.2016.05.002.

[41] J. Pegues, M. Roach, R. Scott Williamson, N. Shamsaei, Surface roughness effects on the fatigue strength of additively manufactured Ti-6Al-4V, Int. J. Fatigue. 116 (2018) 543–552. https://doi.org/10.1016/j.ijfatigue.2018.07.013.